ACS Sustainable Chemistry & Engineering

Research Article

pubs.acs.org/journal/ascecg

# Phytosynthesis of Au, Ag, and Au–Ag Bimetallic Nanoparticles Using Aqueous Extract of Sago Pondweed (*Potamogeton pectinatus* L.)

Ayman A. AbdelHamid,[†] Medhat A. Al-Ghobashy,[‡] Manal Fawzy,[§] Mona B. Mohamed,[∥] and Mohamed M.S.A. Abdel-Mottaleb*[,†]

[†] Nanotechnology Centre, Nile University, Smart Village, B2-Km 28, Cairo-Alex Desert Road, Giza 12677, Egypt

[‡] Biotechnology Centre, Faculty of Pharmacy, Cairo University, Cairo, Egypt

[§] Faculty of Science, Environmental Sciences Department, Alexandria University, 21511 Moharram Bek, Alexandria, Egypt

[∥] The National Institute of Laser Enhanced Sciences, Cairo University, Cairo, Egypt

Supporting Information

**ABSTRACT:** A green and facile method for the synthesis of Au, Ag, and Au–Ag bimetallic nanoparticles was developed using the aqueous extract of sago pondweed (*Potamogeton pectinatus* L.). Size, morphology, crystallinity, composition, capping layer, and stability of the synthesized nanoparticles were all investigated. The effect of the synthesis variables on the nanoparticles was also studied. Results showed that the synthesized nanoparticles were mostly spherical in shape, although other shapes as nanotriangles and hexagons were occasionally observed. Alloy-type Au–Ag nanoparticles could be synthesized at pH 12. The synthesis of the nanoparticles was optimized. The synthesized nanoparticles were stable over three weeks. Results indicate that the flavones and proteins present in the plant extract are responsible for the synthesis and stabilization of the nanoparticles.

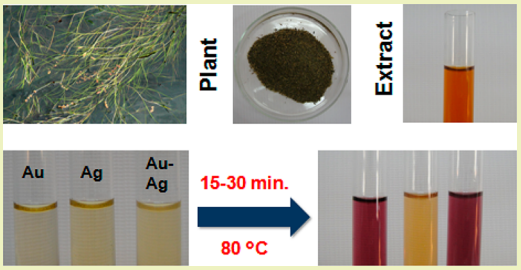


**KEYWORDS:** *Green synthesis, Biosynthesis, Gold nanoparticles, Silver nanoparticles, Alloy, Surface plasmon resonance, Fennel pondweed, Flavones*

## INTRODUCTION

Gold and silver nanoparticles are used in various applications such as biomedical devices, biosensors,[1] catalysis, electronics[2] and pharmaceuticals.[3] Bimetallic nanoparticles are important especially in catalysis, where they have shown better catalytic activity than the monometallic ones of the same elements.[4−6] Au–Ag alloy nanoparticles are specifically utilized for the oxidation of carbon monoxide at low temperature and the oxidation of alcohol aerobically;[7] in addition, they allow tuning the optical properties of the nanoparticles by changing the ratio of the precursor salts.[8] However, many synthesis methods of alloy-type bimetallic nanoparticles suffer from phase separation that occurs at the atomic level leading to the formation of core–shell particles.[7,9] Special capping agents as oleylamine and poly(vinyl pyrrolidone) are also required in most of these methods.[10]

Many chemical and physical processes are currently used for fabrication of metal nanoparticles such as chemical reduction,[11] electrochemical synthesis,[12] photochemical reduction,[13] laser ablation,[14] UV irradiation,[15] lithography,[16] and pyrolysis.[17] However, these methods are expensive and/or may be environmentally hazardous.[18−21] Several reducing and stabilizing agents are used in the chemical synthesis of the metal nanoparticles such as sodium citrate,[11] sodium borohydride,[22] hydrazine,[23] hydroxylamine,[24] and tetrakis(hydroxymethyl)-phosphonium choride (THPC).[25] Many of these materials are not suitable for critical applications such as in medicine. Furthermore, they represent an environmental hazard.[1−3,20]

Eco-friendly methods for the synthesis of metal nanoparticles are needed to avoid or minimize such problems.[26] Many studies have investigated the biosynthesis of metal nanoparticles. Some of them used microorganisms such as bacteria,[27] actinomycetes,[28] and fungi,[29] while others used whole plants.[30−33] However, these methods have limitations such as the difficulty of implementation on a large scale and the need for maintaining cell cultures in the case of using microorganisms.[1,34]

Plant extracts and derivatives have been intensively studied for the synthesis of metal nanoparticles because this approach is simple, practical, and scalable.[34] Many studies have reported using leaves,[3,35−40] seeds,[37,41] latex,[42,43] gum,[1] stems, roots,[44] and fruits.[45] In addition, some plant extracts such as *Swietenia mahogani* JACQ. leaf extract[2] and *Azadirachta indica* leaf broth[31] were successfully used to synthesize bimetallic nanoparticles. However, only a few studies have managed to phytosynthesize alloy-type metal nanoparticles and confirm their alloy nature.[2,4,10,46,47]

*Potamogeton pectinatus* L. (Po) is a cosmopolitan submerged macrophyte that is widely distributed.[48−50] The main

Received: March 30, 2013
Revised: August 31, 2013
Published: September 30, 2013

  

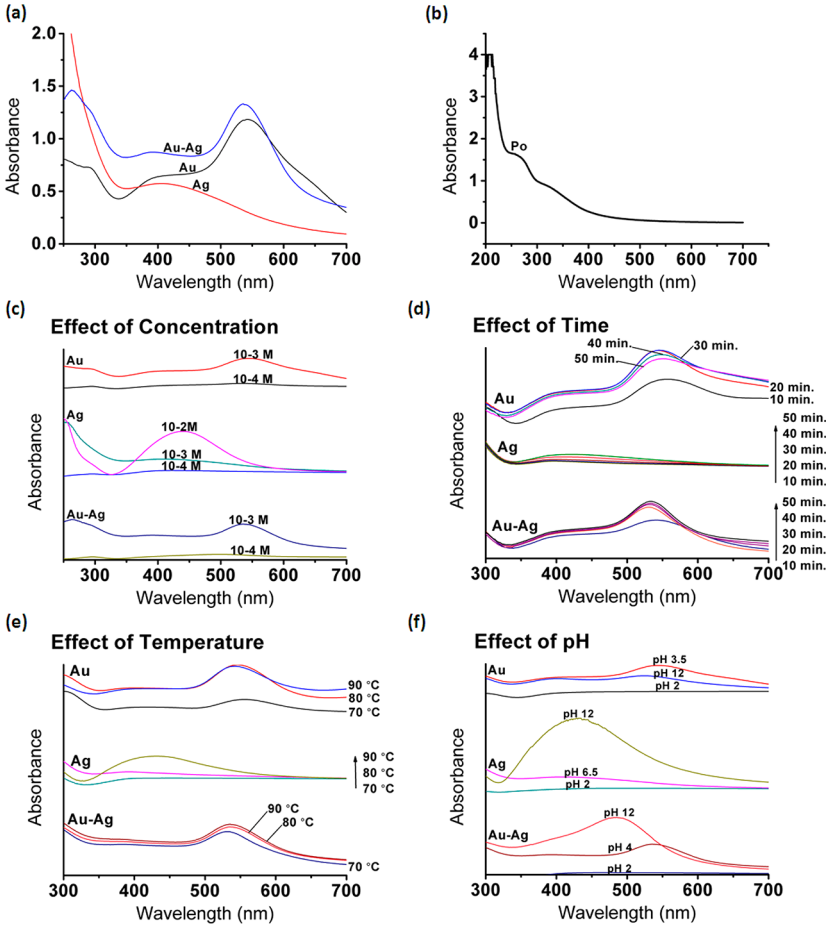


**Figure 1.** UV−vis absorbance spectra of Au, Ag, and Au−Ag (1:1) nanoparticles (a). UV−vis spectrum of Po aqueous extract (b). Effect of concentration of precursor salt(s) (c), reaction time (d), temperature (e), and pH (f) on SPR of the metal nanoparticles.

phytochemicals in Po are flavones and their glycosylated derivatives, labdane diterpenes[51] and proteins.[50] The main flavone is luteolin; apigenin and chrysoeriol exist in lower amounts.[51] Polyphenolic compounds especially flavonoids have been previously reported to be involved in the reduction of the metal ions into metal nanoparticles, and this was attributed to the ability of the flavonoids to chelate metal ions and donate electrons and hydrogen atoms.[19,37,44,52−54] Proteins were also reported to be active in the synthesis and stabilization of metal nanoparticles owing to the amine and carboxylate residues[41,46,52,55,56] and the carbonyl groups that bind strongly to the metal surface acting as capping and stabilizing molecules.[1,52,57] Although Po has high potential for the synthesis of metal nanoparticles, this has not been previously reported.

In this paper, we report on a green and facile method for the synthesis of Au, Ag, and Au−Ag bimetallic nanoparticles using the aqueous extract of Po. We also show that the Au−Ag nanoparticles synthesized at pH 12 are of an alloy type. This is the first report on using Po for the phytosynthesis of metal nanoparticles and is among the few studies that confirmed the alloy nature of the phytosynthesized bimetallic nanoparticles. These metal nanoparticles can be used in various applications such as catalysis and biomedical purposes.

## MATERIALS AND METHODS

**Materials.** *Potamogeton pectinatus* L. was collected from Lake Marriott, which is one of the Nile Delta Lakes in Southern Alexandria, Egypt, in the spring of 2010. Samples were immediately transferred to the lab, washed thoroughly with deionized water twice, then dried in oven at 60 °C until constant weight. The dry biomass was then ground in a stainless steel grinder and sieved. Hydrogen tetrachloroaurate monohydrate ($HAuCl_4 \cdot H_2O$) was purchased from Electron Microscopy Sciences, U.S.A.; silver nitrate was purchased from Sigma-Aldrich, U.S.A. All chemicals were used as purchased.

**Preparation of Aqueous Extract of *Potamogeton pectinatus* L.** Fine powdered *Potamogeton pectinatus* L. plant (1.5 g) was placed in 250 mL Erlenmeyer flask containing 30 mL distilled water, and then heated at 80 °C while stirring for 10 min. This was followed by centrifugation at 4000 rpm for 15 min, and the supernatant was then filtered using two superimposed filter papers. The extract was stored in the refrigerator at 4 °C for further use. The prepared extract was used within one week of preparation.

**Determination of Total Phenolic Content in Po Aqueous Extract.** The Folin-Ciocalteu (FC) assay was used for the determination of the total phenolic content of the aqueous extract.[58] This assay can also be considered as a measure of the total antioxidant capacity of the extract.[59] The aim of using this assay is to standardize the amount of polyphenols and other potential reducing agents in the Po extract when different batches are used. The assay was conducted according to the method of Ferreira et al.[60] with some modifications. Briefly, a 1 mL aliquot of the aqueous Po extract was mixed with 7.5 mL of 0.2 M NaOH in a 25 mL volumetric flask, and then 3.5 mL of FC reagent (diluted 7 folds using distilled water) was added. The solution was mixed by gentle shaking and incubated for 60 min in the dark at room temperature. It was then completed to 25 mL using distilled water, and the absorbance was measured at 750 nm. A blank was prepared using the same procedure; however, distilled water was used instead of the extract. Gallic acid was used to prepare the


dx.doi.org/10.1021/sc4000972 | ACS Sustainable Chem. Eng. 2013, 1, 1520−1529

calibration curve, and the assay results were expressed in terms of μg gallic acid equivalents/mL of the aqueous extract.

**Synthesis and Stability of Metal Nanoparticles.** An aliquot (1.5 mL) of the Po extract was added to 15 mL of $10^{-3}$ M $HAuCl_4 \cdot H_2O$, $AgNO_3$, and $HAuCl_4.H_2O + AgNO_3$ (1:1 molar ratio) for the synthesis of Au, Ag, and Au−Ag bimetallic nanoparticles, respectively. The solution was then heated on a hot plate at 80 °C for 15 min in the case of Au nanoparticles and 30 min in the cases of Ag and Au−Ag bimetallic nanoparticles. Experiments were repeated twice. These are the initial synthesis conditions, and they were used in this study unless otherwise stated. The synthesized nanoparticles were refrigerated at 4 °C. UV−vis absorbance was measured periodically for three weeks to assess the stability of the nanoparticles.

**Studying the Effect of Synthesis Variables on Synthesized Metal Nanoparticles.** Different concentrations ($10^{-2}$, $10^{-3}$, and $10^{-4}$ M) of the precursor salt(s), reaction times (10, 20, 30, 40, and 50 min), temperatures (70, 80, and 90 °C), and pH conditions (nonadjusted reaction pH, pH 2, and pH 12) were used to prepare Au, Ag, and Au:Ag (1:1) nanoparticles. Dilute HCl and NaOH were used for pH adjustment. Au−Ag bimetallic nanoparticles were synthesized using $HAuCl_4 \cdot H_2O$:$AgNO_3$ (0:1, 1:3, 1:1, 3:1, 1:0 molar ratios) at pH 12 to study the effect of the Au:Ag molar ratio on the Au−Ag bimetallic nanoparticle composition. Experiments were repeated twice, and average values were reported.

**Characterization.** An UV−visible (UV−vis) spectrophotometer (SHIMADZU model UV-1650 PC, Japan) was used for absorbance measurement. Transmission electron microscopy (TEM) and selected area electron diffraction (SAED) analysis were carried out using a JEOL JEM-2100 instrument (Japan) that was operated at 200 kV; samples were prepared by dipping the carbon-coated copper grids in the prepared solutions for 5 min and then leaving them to dry on a filter paper. More than 200 nanoparticles were used to determine the size distribution and the average size of the synthesized nanoparticles. An energy dispersive X-ray spectroscopy (EDX) detector (Oxford Instruments, U.K.) attached to scanning electron microscope (JEOL JSM-5300, Japan) was used to determine the elemental composition of the metal nanoparticles; samples were prepared by centrifugation at 13,000 rpm and redispersion in distilled water 3 times to remove free ions, followed by drying. X-ray diffraction (XRD) was carried out on unwashed dried samples using a Philips analytical X-ray diffractometer (X'pert). Fourier transform infrared spectroscopy (FTIR) was done using a Nicolet 6700 FTIR instrument (Thermo Scientific, U.S.A.). Zeta potential was measured using a Zetasizer Nano ZS-ZEN 3600 (Malvern Instruments Ltd., U.K.).

## RESULTS AND DISCUSSION

**UV−Vis Spectral Analysis.** Gold and silver nanoparticles are known to exhibit surface plasmon resonance (SPR) phenomenon, where conducting electrons in metals oscillate collectively in resonance with certain wavelengths upon interaction with an electromagnetic field.[36] SPR band depends on the type, size, shape of the nanoparticles, and the surrounding environment.[61] Such specific SPR bands were used to detect the synthesis of metal nanoparticles.

Au nanoparticles were successfully synthesized after heating for 15 min; the colloid had a dark purple color and a SPR peak at 542.5 nm. Ag nanoparticles were formed after 30 min, had a light brown color, and a SPR peak at 406.0 nm (Figure 1a). However, the SPR band of Ag nanoparticles was of a much lower intensity than that of the Au nanoparticles. The lower intensity is due to the lower yield of Ag nanoparticles. The longer synthesis time and lower yield may be attributed to the faster reduction rate of $Au^{3+}$ as a result of the higher reduction potential of $Au^{3+}/Au$ than $Ag^+/Ag$.[3,31,34,62] Au−Ag (1:1) bimetallic nanoparticles were synthesized after 30 min to ensure reduction of both metal ions. The Au−Ag (1:1) colloid had a magenta color and SPR band at 536.0 nm (Figure 1a). The concentrations of $Au^{3+}$ and $Ag^+$ in the Au−Ag (1:1) nanoparticles synthesis reaction are half of those in the Au and Ag nanoparticles synthesis reactions. Nevertheless, it was noticed that the color of the Au−Ag (1:1) colloid appeared after ∼5−10 min. This is faster than the appearance of the color of the Au colloid after ∼15 min and of the Ag colloid after ∼30 min. This fast appearance of color can be explained by the acceleration of the reduction of $Au^{3+}$ in the presence of $Ag^+$.[31]

The UV−vis spectrum of the Po aqueous extract (Figure 1b) showed strong absorption at ∼208.0 nm and an absorbance peak at ∼270.0 nm, which indicate the presence of peptide bonds and (tryptophan, tyrosine, and/or phenylalanine residues), respectively.[45,50]

**Stability Study.** The metal nanoparticles have shown excellent stability over three weeks (Figure S1, Supporting Information); the UV−vis spectra did not show significant changes in $\lambda_{max}$ (wavelength at which maximum absorbance occurs) or full width at half-maximum (FWHM: a measure of the homogeneity of nanoparticles)[63] over time, indicating stable particle size and size distribution. However, a slight increase in SPR peak intensity was observed especially in the cases Ag and Au−Ag nanoparticles. This can be explained by the formation of new nanoparticles over time.

**Effect of the Synthesis Variables on Metal Nanoparticles.** The synthesis procedure of metal nanoparticles was optimized by controlling synthesis variables. The effect of concentration of metal precursor(s), reaction time, temperature, and pH has been studied.

Au nanoparticles were successfully synthesized using $10^{-3}$ and $10^{-4}$ M of $HAuCl_4 \cdot H_2O$. However, when $10^{-2}$ M of the salt was used, precipitation occurred, where the solution turned colorless with large dispersed particles. The SPR band of the Au-$10^{-3}$ nanoparticles was of much higher intensity than that of Au-$10^{-4}$. Au-$10^{-3}$ also had a higher $\lambda_{max}$ (545.0 nm) compared to that of that of Au-$10^{-4}$, which was at 534.5 nm (Figure 1c). This shows an increase in the yield and size of the nanoparticles at higher concentration. This is due to the abundance of $Au^{3+}$ ions in the solution causing more nucleation and also fueling growth of the nanoparticles.

Ag-$10^{-4}$ did not show a detectable SPR band, indicating very low yield of nanoparticles formed; however, Ag-$10^{-3}$ and Ag-$10^{-2}$ have shown detectable bands with $\lambda_{max}$ at 410.0 and 439.5 nm, respectively (Figure 1c). The intensity of the SPR band of Ag-$10^{-2}$ was much higher than that of Ag-$10^{-3}$. Ag nanoparticles show a similar trend to Au. However, the absence of aggregation of Ag nanoparticles at high concentration ($10^{-2}$ M $AgNO_3$) and very low yield at low concentration ($10^{-4}$ M $AgNO_3$) may be attributed to the low reduction rate of $Ag^+$.

Au−Ag (1:1) bimetallic nanoparticles could not be formed at a concentration of $10^{-2}$ M of the precursor salts because of the large amount of AgCl precipitate formed upon mixing the salts together. The SPR band intensity of Au−Ag-$10^{-3}$ was much higher than that of Au−Ag-$10^{-4}$, it also had a larger $\lambda_{max}$ (535.5 nm) compared to that of Au−Ag-$10^{-4}$, which was 498.5 nm (Figure 1c). Thus, the behavior of Au−Ag (1:1) is coherent with that of Au and Ag. However, the increase in $\lambda_{max}$ may also be related to the ratio of Au to Ag in the bimetallic nanoparticles, which affects the position of the SPR in the spectrum. This will be explained later.

The increase in reaction time resulted in an increase in the SPR intensity of the metal nanoparticles (Figure 1d). It was noticed that the SPR peaks of Au and Au−Ag (1:1) nanoparticles became sharper in the time period between 10

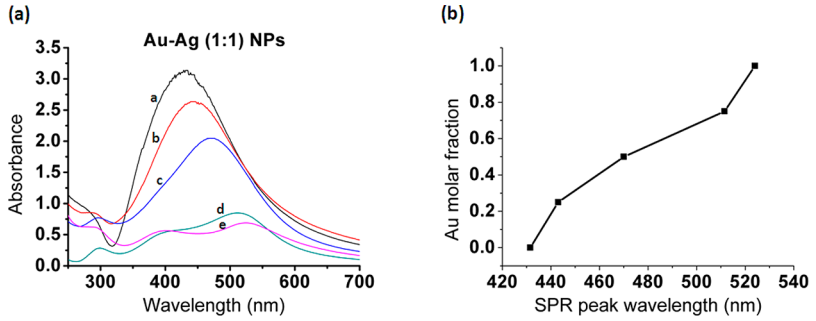


**Figure 2.** Effect of Au:Ag molar ratio on SPR of Au–Ag bimetallic nanoparticles synthesized at pH 12 (a). Relationship between Au molar fraction and SPR $\lambda_{max}$ of Au–Ag bimetallic nanoparticles synthesized at pH 12 (b).

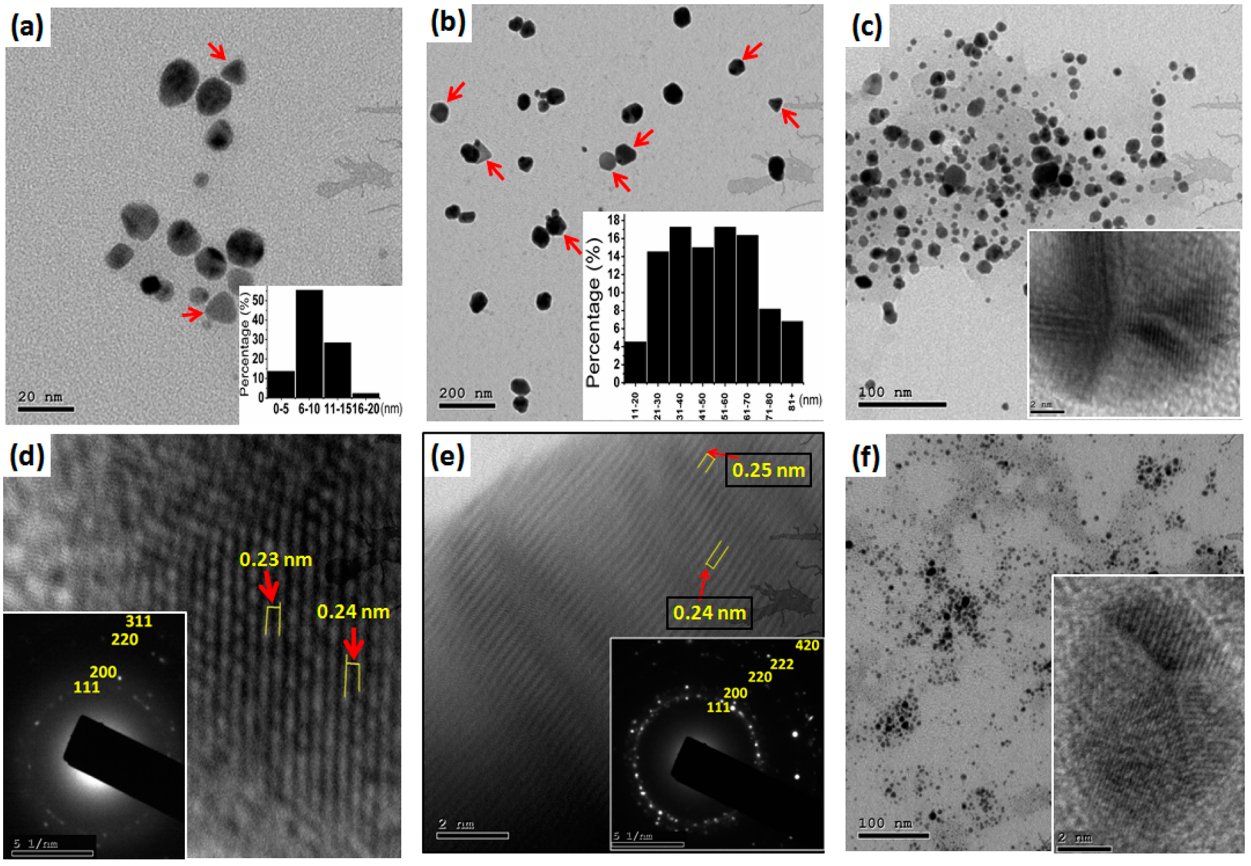


**Figure 3.** TEM image and size distribution (inset) (a) and HRTEM image/SAED pattern (d) of Au nanoparticles. TEM image and size distribution (inset) (b) and HRTEM image/SAED pattern (e) of Ag nanoparticles. Arrows in (a,b) point to triangular and hexagonal nanoparticles. TEM and HRTEM (inset) images of Au–Ag (1:1) nanoparticles synthesized at pH 4 (c) and pH 12 (f).

and 20 min, indicating that the nanoparticles became more homogeneous after 20 min. No major increase in the SPR intensity was observed after 20 min in the cases of Au and Au–Ag (1:1) nanoparticles. On the contrary, Au nanoparticles seem to undergo precipitation after 30 min, which is evident from the decrease in the SPR intensity. Visible precipitation of Au nanoparticles was evident. Ag nanoparticles behaved differently, where the SPR intensity increased steadily, and the SPR wavelength red-shifted; indicating an increase in the yield and particle size respectively. This shows that the Ag nanoparticles were still growing even after 50 min. This may be due to the slow reduction of $Ag^+$.

Temperature increase resulted in an increase in the yield of the nanoparticles (Figure 1e). This is expected due to the increase in the reaction rate. However, it was observed that a slight decrease in SPR band intensity occurred at 90 °C in the cases of Au and Au–Ag (1:1) nanoparticles; this indicates reaction saturation and may show a tendency for precipitation upon further heating. It was noted that Ag nanoparticles were not formed at 70 °C. SPR of Ag nanoparticles showed a significant shift to a longer wavelength at 90 °C, indicating an increase in the size of the nanoparticles. The different behavior of Ag nanoparticles may be due to the slower reduction of $Ag^+$.

Acidic pH (pH 2) was not suitable for the synthesis of any of the nanoparticles. However, they were readily formed without pH adjustment and at pH 12 (Figure 1f). The reaction pH without adjustment was 3.5, 6.5, and 4 in the cases of Au, Ag, and Au–Ag (1:1) nanoparticles, respectively. In the case of Au nanoparticles, SPR band intensity and wavelength were low at


dx.doi.org/10.1021/sc4000972 | ACS Sustainable Chem. Eng. 2013, 1, 1520–1529

pH 12, indicating a smaller particle size and lower yield. pH 3.5 was the optimum pH for the synthesis of Au nanoparticles.

Ag nanoparticles showed moderate SPR intensity with $\lambda_{max}$ at 410.0 nm at pH 6.5. At pH 12, nanoparticles were formed at a much faster rate, and a high intensity SPR band appeared at 431.5 nm. This shows that pH 12 induces more nucleation and growth of Ag nanoparticles, which could be attributed to the activation of the phytochemicals involved in their synthesis in alkaline conditions.

Au−Ag nanoparticles also had a higher SPR peak intensity at pH 12, but its wavelength blue-shifted from 536 nm at pH 4 to 483.5 nm at pH 12. This can be explained by the more efficient reduction of $Ag^+$ at pH 12, thus causing the SPR band to appear closer to the SPR band of Ag nanoparticles.

The optimum pH for the synthesis of Au nanoparticles is different from that of Ag and Au−Ag bimetallic nanoparticles. This may be attributed to different phytochemicals being responsible for their synthesis.

**Optimized Conditions for Synthesis of Metal Nanoparticles.** On the basis of the results obtained, the synthesis conditions could be optimized. The recommended conditions varied according to the type of target nanoparticle. The synthesis of Au nanoparticles was optimum at a concentration of $HAuCl_4 \cdot H_2O$ of $10^{-3}$ M and heating at 80 °C for 15−20 min without adjusting the pH (pH 3.5). For Au−Ag (1:1) nanoparticles, the synthesis was optimum at a concentration of $10^{-3}$ M of $HAuCl_4 \cdot H_2O$ + $AgNO_3$ and heating at 80 °C for 30 min at pH 12. For Ag nanoparticles, heating at 90 °C for 30 min or more at pH 12 and using a concentration of $AgNO_3$ from $10^{-3}$ to $10^{-2}$ M was optimum.

The total phenolic content of the first batch of the Po extract contained 7.4 μg gallic acid equivalents/mL of extract, and 1.5 mL was used for the synthesis of the nanoparticles. Therefore, the volumes of other batches of Po extract were adjusted, so that a total amount of 11.1 μg of gallic acid equivalents is used in each experiment.

**Effect of Au:Ag Molar Ratio on Au−Ag Bimetallic Nanoparticles.** Au−Ag nanoparticles at different Au:Ag molar ratios were synthesized at pH 12 to investigate the nature of the nanoparticles. The SPR peaks of Au:Ag (1:0), (3:1), (1:1), (1:3), and (0:1) were 524.0, 511.5, 470.0, 443.0, and 431.5 nm, respectively (Figure 2a). Only one SPR peak appeared; it was positioned between those of the pure metal nanoparticles and red-shifted as the Au molar ratio increased in a quasi-linear relationship (Figure 2b). This shows that the Au−Ag bimetallic nanoparticles synthesized at pH 12 are of an alloy type and not a physical mixture or core−shell.[2,5,7,10,46,47,64] Alloy-type nanoparticles are formed due to the similar lattice structures of Au and Ag that allow their miscibility in a homogeneous alloy.[5] It was also noticed that the SPR peak intensity decreased as the Au molar ratio increased indicating that the alkaline medium is not favorable for the reduction of $Au^{3+}$; this agrees with our previous results in this study.

**TEM Analysis.** The morphology of the nanoparticles was visualized using TEM. Au nanoparticles were spherical in shape, although a few nanotriangles existed as well (Figure 3a, Figure S2a, Supporting Information). It could be also seen that the nanoparticles are well separated from each other indicating good capping and the absence of aggregation. The nanoparticles had an average size of 8.4 ± 3 nm (Figure 3a, inset). High resolution TEM (HRTEM) has shown some of the nanoparticles to be multiple twinned; it has also revealed clear lattice fringes with fringe spacing of 0.239 ± 0.009 nm (Figure 3d) that matches the (111) plane of the Au crystal lattice (JCPDS card No: 04-0784). SAED analysis of one of the nanoparticles showed concentric diffraction rings that indicated the polycrystalline nature of the nanoparticles. The *d*-spacings determined from the SAED pattern (Figure 3d, inset) were 2.37, 2.04, 1.44, 1.22, and they could be indexed as (111), (200), (220), and (311) reflections, respectively, (JCPDS card No: 04-0784) that correspond to face centered cubic (fcc) Au.

TEM showed a low yield of Ag nanoparticles (in agreement with the low intensity SPR peak). Thus a higher concentration of $AgNO_3$ ($3 \times 10^{-3}$ M) was used for the synthesis of Ag nanoparticles to allow the study of their morphology. The synthesized nanoparticles were mostly spherical in shape; however, hexagons, triangles, and truncated triangles could be seen as well (Figure 3b, Figure S2b,c,d, Supporting Information). These anisotropic silver nanoparticles are favored for some applications such as surface enhanced Raman scattering (SERS) spectroscopy.[65] HRTEM showed that the particles have multiple-twinned polyhedral morphology. Coalescence of some nanoparticles was observed. In addition, nanotriangles appeared with blunt angles, and both of these phenomena occur to minimize surface free energy.[19,56,65] However, they are different from the conglomerates seen in high density areas that could be due to interaction between the capping biomolecules.[19] Ag nanoparticles were polydispersed with an average size of 50.4 ± 21.8 nm (Figure 3b, inset). This large size may be due to the higher concentration of $AgNO_3$ salt utilized in the synthesis of the nanoparticles; this is in accordance with our previous results showing the effect of concentration on particle size. The polydispersity may be due to the formation of the nanoparticles at different times during synthesis, accompanied by their continuous growth due to the high concentration of $AgNO_3$ used. The fringe spacing could be determined from the HRTEM to be 0.232 ± 0.008 nm (Figure 3e) that matches the (111) plane of Ag crystal lattice (JCPDS card No: 04-0783). SAED (Figure 3e, inset) revealed concentric diffraction rings with *d*-spacings of 2.34, 2.05, 1.41, 1.19, and 0.92 that could be indexed as (111), (200), (220), (222), and (420) reflections, respectively, (JCPDS card No: 04-0783). These planes correspond to fcc Ag.

TEM images were taken for Au−Ag (1:1) nanoparticles at pH 4 and pH 12. At pH 4, the nanoparticles appeared to have polygonal shapes, where hexagons and polyhedrons were abundant; in addition, nanotriangles with blunt edges were seen. Fusion of some of the particles was noticed (Figure 3c). The average size of the nanoparticles was 10.6 ± 5.0 nm (Figure S2e, Supporting Information). SAED pattern of one of the particles showed that the nanoparticles have a polycrystalline nature (data not shown).

At pH 12, the nanoparticles were mostly spherical (Figure 3f, Figure S2f, Supporting Information); however, HRTEM images showed that they have multiple-twinned octahedral shape as in the case of pH 4 (Figure 3f, inset). The higher yield agrees with the UV−vis results. The average nanoparticle size was 6.6 ± 2.4 nm (Figure S2f, inset, Supporting Information). The small uniform particle size may be due to the high reduction rate at pH 12. SAED pattern shows that the nanoparticles have a polycrystalline nature (data not shown).

TEM images of the metal nanoparticles clearly show a light-colored layer coating the nanoparticles (Figure S2d, Supporting Information). This is due to the biomolecules that surround the nanoparticles and act as a protective barrier against aggregation.

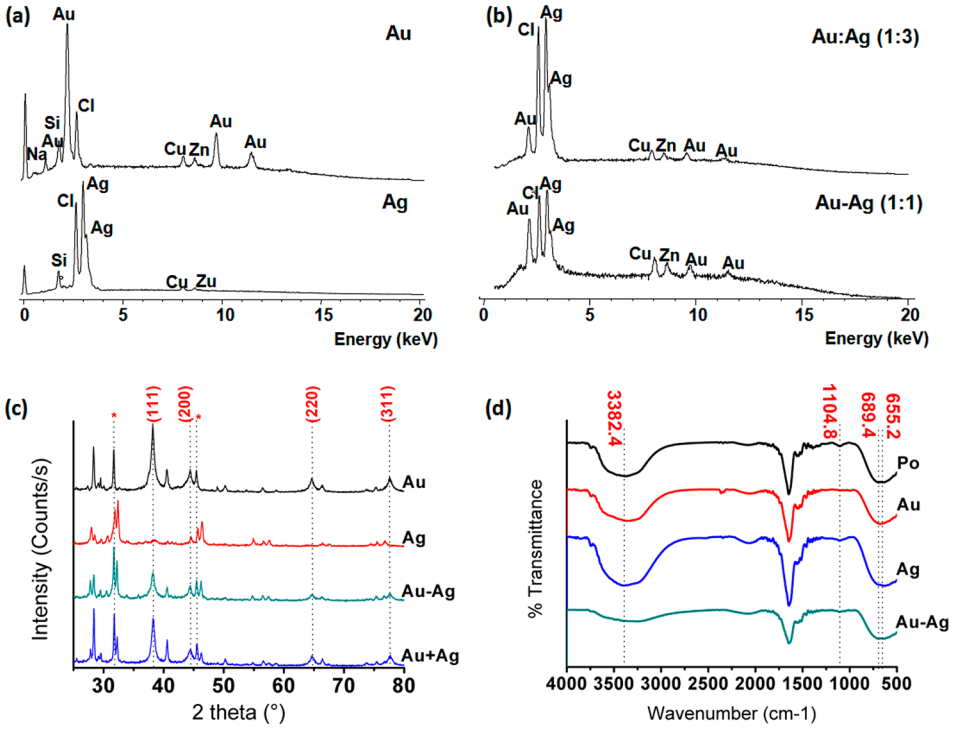


**Figure 4.** EDX spectra of Au and Ag nanoparticles (a). Au–Ag (1:3)/(1:1) nanoparticles synthesized at pH 12 (b). XRD patterns of the metal nanoparticles (c). (∗) denotes unassigned peaks that may be of biocrystalline origin. FTIR spectra of Po aqueous extract and the metal nanoparticles (d).

The appearance of this capping organic layer surrounding metal nanoparticles has been previously reported.[19,31,44,45,66]

**EDX Analysis.** EDX was carried out to determine the elemental composition of the synthesized metal nanoparticles. Au and Ag nanoparticles showed strong signals of Au and Ag, respectively; however, weak background signals were seen as well (Figure 4a). The weak signals represented Cu, Zn, Cl, Na, P, and Si; Cu may be due to the copper grids used in the analysis, while the rest of the elements may be due to the biomolecules that are capping the nanoparticles. The absorption peak of Ag nanoparticles is around 3 KeV, which is in accordance with the previously reported value, and this has been attributed to SPR.[42]

EDX of Au–Ag (1:1, 1:3) nanoparticles prepared at pH 12 have shown strong peaks of Au and Ag in addition to weaker signals of Cu, Cl, and Zn (Figure 4b). EDX is a semi-quantitative technique, we could use it to determine the Au:Ag molar ratio within the nanoparticles. It was found that the Au:Ag molar ratio was ∼1:1.1 in Au–Ag (1:1) nanoparticles and ∼1:2.8 in Au–Ag (1:3) nanoparticles. This shows that the molar ratio of the precursor salts was maintained after synthesis.

It was noticed that the percentage of Cl is high in the case of Ag nanoparticles, and it increased with the increase of the ratio of Ag in the case of Au–Ag bimetallic nanoparticles. This can be explained by the formation of AgCl crystals as previously reported.[67]

**XRD Analysis.** XRD analysis has been carried out to study the crystal structure of the biosynthesized metal nanoparticles (Figure 4c). In the case of Au nanoparticles, the Bragg reflection peaks appeared at positions 38.2°, 44.4°, 64.6°, and 77.6° that correspond to interplanar spacings of 2.35, 2.04, 1.44, and 1.23 Å, respectively, and could be indexed to (111), (200), (220), (311) lattice planes of fcc Au, respectively, (JCPDS file 04-0784). This is in accordance with SAED results. The presence of highly crystalline KCl phase (JCPDS file 41-1476) was noticed, where its peaks are prominent in the XRD pattern. In addition, there are unassigned peaks that may be due to crystals of bio-organic phase as previously observed.[55,65,68] The ratio of the intensity of the diffraction peak corresponding to (200) crystallographic plane to that corresponding to (111) plane was found to be 0.36, which is much lower than the conventional bulk ratio (0.52).[36,55] This indicates that (111) is the predominant crystallographic plane in the Au nanoparticles. The (111) facet is known to be more reactive because it has high atom density.[69]

The broadened Bragg's peaks show that nanoparticles were formed.[46,53] The mean crystallite size was calculated using Debye–Scherrer's equation (eq 1)

$$D = K\lambda/\beta_s \cos\theta \quad (1)$$

where $D$ is the average particle size, $K$ is the shape dependent Scherrer's constant, $\lambda$ is the X-ray wavelength, $\beta_s$ is FWHM of the diffraction peak of plane (111), and $\theta$ is the diffraction angle.[46,67] The mean size of Au nanoparticles was calculated to be 11.8 nm, which is close to the average particle size determined using TEM (8.4 nm ±3 nm). However, the TEM measurement is considered to be more accurate as polydispersity, and shape variation may cause inaccuracy in the Debye–Scherrer's equation.[53]

The Bragg diffraction peaks of Ag nanoparticles appeared at positions 38.67°, 44.56°, 66.42°, and 76.79° that are corresponding to $d$-spacings of 2.33, 2.03, 1.41, and 1.24 Å, respectively, and could be indexed to (111), (200), (220), and (311) planes of fcc Ag, respectively, (JCPDS card No: 04-0783). However, the peaks are weak with respect to other peaks that represent AgCl (JCPDS card No: 31-1238), KCl, and AgO (JCPDS card No: 43-1038) crystals. This is due to the very low yield of Ag nanoparticles under the initial conditions as


dx.doi.org/10.1021/sc4000972 | ACS Sustainable Chem. Eng. 2013, 1, 1520–1529

previously mentioned. Other unassigned peaks that may represent bio-organic phase crystals also appeared.

XRD patterns of Au−Ag (1:1) nanoparticles at pH 4 and a physical mixture of phytosynthesized Au and Ag nanoparticles showed no significant difference. This is expected due to the close crystal lattice structures of Au and Ag. The Bragg reflection peaks could be indexed to (111), (200), (220), and (311) planes; the broadened peaks indicate the formation of nanoparticles. Several peaks corresponding to AgCl (JCPDS card No: 31-1238), KCl, and AgO (JCPDS card No: 43-1038) in addition to unassigned peaks were observed. The ratio of the peak intensity of (200) plane to that of (111) plane in the Au−Ag bimetallic nanoparticles was 0.37, indicating the dominance of the (111) plane. The crystallite size in the case of Au−Ag bimetallic nanoparticles was calculated using Debye−Scherrer's equation to be 13.7 nm, which is close to that determined by TEM (10.6 ± 5 nm).

**FTIR Analysis.** FTIR was carried out to determine the biomolecules that may be responsible for the reduction and capping of the metal nanoparticles (Figure 4d). The IR spectra were determined for the Po extract and for the synthesized nanoparticles. The main peaks that were identified in the IR spectrum of the Po extract were at 3744.4, 3382.4, 2066.4, 1646.6, 1559.0−1542.1, 1421.6−1338.8, 1104.8, and 589.4−655.2 $cm^{-1}$. They may be assigned to free O−H stretching vibration, hydrogen-bonded O−H stretching vibration, C═C asymmetric stretching vibration, amide I band due to the stretching vibration of the C═O in amide bonds, amide II band due to the N−H bending vibrations in amide bonds, C−O−H bending of carboxylic acids or in-plane O−H bending vibrations, C−N or C−O stretching vibrations, and $NH_2$, N−H wagging or out-of-plane O−H bending vibrations, respectively.

In Au, Ag, and Au−Ag (1:1) nanoparticles, the peak at 3382.4 $cm^{-1}$ that was attributed to the hydrogen-bonded O−H stretching vibration in the Po aqueous extract was shifted to 3354.5, 3389.6, and 3255.1 $cm^{-1}$, respectively. Also the peaks at 689.4 and 655.2 $cm^{-1}$ assigned to $NH_2$, N−H wagging or out-of-plane O−H bending vibrations in the Po extract were shifted to 678.3, 631.1, and 696.4 and 634.8 $cm^{-1}$, respectively. It was also noticed that the peak at 1104.8 $cm^{-1}$ that was assigned to C−N or C−O stretching vibrations in Po extract disappeared in the case of Au nanoparticles.

The data mentioned above indicate that O−H, COOH, C═C, C−H, C−N, and amide C═O, and N−H could be present in the Po extract. These functional groups can be assigned to the presence of polyphenolic compounds as flavonoids and also to proteins. The peak changes in the IR spectra of the synthesized metal nanoparticles were related to the OH and $NH_2$ groups indicating that these functional groups are involved in their synthesis and capping.

We suggest that flavones (especially luteolin) that are abundant in the aqueous Po extract are the main components that are responsible for the reduction of the metal ions. In addition, the carboxylic and amine residues of proteins may participate in the reduction process as they are able to donate electrons to the metal ions. Stabilization of the formed nanoparticles can be attributed to the protein components, where the carboxylate, amine, and carbonyl groups can bind to the surface of the metal nanoparticles, thus stabilizing them and preventing their aggregation.

**Zeta Potential Analysis.** Zeta potential of the metal nanoparticles synthesized at unadjusted pH and at pH 12 was measured (Table 1). It was found to be around −30 mV at pH 12 for all samples. However, it decreased to around −19 mV at pH 3.5 and pH 4 for Au and Au−Ag nanoparticles, respectively, and remained almost the same in the case of Ag nanoparticles ($3 \times 10^{-3}$ $AgNO_3$ used in synthesis) at pH 6.5. The increase in zeta potential at alkaline pH may be attributed to the ionization of the hydroxyl and carboxylic groups in the capping moieties, this would increase the negative charge on the surface of the nanoparticles. The high negative charge forms a repulsive barrier that physically separates the nanoparticles. This helps to avoid aggregation and thus improves the stability of the colloid.[19]

**Table 1. Zeta Potential of Au, Ag, and Au−Ag (1:1) Nanoparticles**

| metal nanoparticles | pH during synthesis | zeta potential (mV) |
|---|---|---|
| Au | 3.5 | −18.5 |
| Au | 12 | −30.4 |
| Ag[a] | 6.5 | −27.4 |
| Ag | 12 | −28.7 |
| Au:Ag (1:1) | 4 | −19.8 |
| Au:Ag (1:1) | 12 | −29.2 |

[a] $3 \times 10^{-3}$ M $AgNO_3$ was used in synthesis

Phytosynthesized Au and Ag nanoparticles are promising materials in various fields due to their catalytic,[70−72] antibacterial,[73−75] larvicidal,[76,77] and electrochemical[78] properties. Au−Ag alloy nanoparticles are promising catalysts. They were reported to have high synergistic catalytic activity.[79,80] CO oxidation using Au−Ag alloy nanoparticles was specifically studied, and the Au−Ag synergistic catalysis was explained. It was found that the electronic properties of Au and Ag are altered by alloying leading to higher tendency to lose electrons, thus enhancing $O_2$ activation. In addition, CO and $O_2$ co-adsorption is improved by alloying.[81,82] Our Au−Ag alloy nanoparticles have high potential for such application. They are also free from toxic surfactants and reducing agents and thus environmentally friendly.

In conclusion, a green and facile method was used to synthesize Au, Ag, and Au−Ag bimetallic nanoparticles using the aqueous extract of sago pondweed (Po). It is the first report of using Po in metal nanoparticle synthesis. The alloy nature of Au−Ag bimetallic nanoparticles (pH 12) was confirmed. The factors affecting the synthesis of the metal nanoparticles were studied and optimized. Flavones and proteins are thought to be responsible for the synthesis and stabilization of the nanoparticles.

## ■ ASSOCIATED CONTENT

### Supporting Information

Figure S1: Effect of storage time on SPR of the metal nanoparticles. Figure S2: TEM images of Au and Ag nanoparticles. HRTEM image of a Ag nanoparticle showing its biocoating (pointed to by the red arrow). Size distribution of Au−Ag (1:1) nanoparticles. This material is available free of charge via the Internet at http://pubs.acs.org.

## ■ AUTHOR INFORMATION

### Corresponding Author

*E-mail: mabdel-mottaleb@nileuniversity.edu.eg.

### Notes

The authors declare no competing financial interest.

## ■ ACKNOWLEDGMENTS

The authors acknowledge Nile University for funding, Nanotech Egypt for Photoelectronics, and The Biotechnology Center, Faculty of Pharmacy, Cairo University in which the experimental work was done. We are also pleased to acknowledge Ahmed Hafez, Faculty of Pharmacy, Cairo University for helping with the zeta potential analysis.

## ■ REFERENCES

(1) Vinod, V. T. P.; Saravanan, P.; Sreedhar, B.; Devi, D. K.; Sashidhar, R. B. A facile synthesis and characterization of Ag, Au and Pt nanoparticles using a natural hydrocolloid gum kondagogu (*Cochlospermum gossypium*). *Colloids Surf., B* **2011**, *83* (2), 291−298.

(2) Mondal, S.; Roy, N.; Laskar, R. A.; Sk, I.; Basu, S.; Mandal, D.; Begum, N. A. Biogenic synthesis of Ag, Au and bimetallic Au/Ag alloy nanoparticles using aqueous extract of mahogany (*Swietenia mahogani* JACQ.) leaves. *Colloids Surf., B* **2011**, *82* (2), 497−504.

(3) Begum, N. A.; Mondal, S.; Basu, S.; Laskar, R. A.; Mandal, D. Biogenic synthesis of Au and Ag nanoparticles using aqueous solutions of black tea leaf extracts. *Colloids Surf., B* **2009**, *71* (1), 113−118.

(4) Zhan, G.; Huang, J.; Du, M.; Abdul-Rauf, I.; Ma, Y.; Li, Q. Green synthesis of Au−Pd bimetallic nanoparticles: Single-step bioreduction method with plant extract. *Mater. Lett.* **2011**, *65* (19−20), 2989−2991.

(5) Senapati, S.; Ahmad, A.; Khan, M. I.; Sastry, M.; Kumar, R. Extracellular biosynthesis of bimetallic Au−Ag alloy nanoparticles. *Small* **2005**, *1* (5), 517−520.

(6) Toshima, N.; Yonezawa, T. Bimetallic nanoparticles—Novel materials for chemical and physical applications. *New J. Chem.* **1998**, *22* (11), 1179−1201.

(7) Sánchez-Ramírez, J. F.; Pal, U.; Nolasco-Hernández, L.; Mendoza-Álvarez, J.; Pescador-Rojas, J. A. Synthesis and optical properties of Au−Ag alloy nanoclusters with controlled composition. *J. Nanomater.* **2008**, *2008*, 9pages.

(8) Hubenthal, F.; Ziegler, T.; Hendrich, C.; Alschinger, M.; Träger, F. Tuning the surface plasmon resonance by preparation of gold-core/silver-shell and alloy nanoparticles. *Eur. Phys. J. D* **2005**, *34* (1−3), 165−168.

(9) Singh, A. V.; Bandgar, B. M.; Kasture, M.; Prasad, B. L. V.; Sastry, M. Synthesis of gold, silver and their alloy nanoparticles using bovine serum albumin as foaming and stabilizing agent. *J. Mater. Chem.* **2005**, *15* (48), 5115−5121.

(10) Zhang, G.; Du, M.; Li, Q.; Li, X.; Huang, J.; Jiang, X.; Sun, D. Green synthesis of Au−Ag alloy nanoparticles using *Cacumen platycladi* extract. *RSC Adv.* **2013**, *3* (6), 1878−1884.

(11) Polte, J.; Ahner, T. T.; Delissen, F.; Sokolov, S.; Emmerling, F.; Thünemann, A. F.; Kraehnert, R. Mechanism of gold nanoparticle formation in the classical citrate synthesis method derived from coupled in situ XANES and SAXS evaluation. *J. Am. Chem. Soc.* **2010**, *132* (4), 1296−1301.

(12) Ma, H.; Yin, B.; Wang, S.; Jiao, Y.; Pan, W.; Huang, S.; Chen, S.; Meng, F. Synthesis of silver and gold nanoparticles by a novel electrochemical method. *ChemPhysChem* **2004**, *5* (1), 68−75.

(13) Lu, H. W.; Liu, S. H.; Wang, X. L.; Qian, X. F.; Yin, J.; Zhu, Z. K. Silver nanocrystals by hyperbranched polyurethane-assisted photochemical reduction of $Ag^{+}$. *Mater. Chem. Phys.* **2003**, *81* (1), 104−107.

(14) Tsuji, T.; Kakita, T.; Tsuji, M. Preparation of nano-size particles of silver with femtosecond laser ablation in water. *Appl. Surf. Sci.* **2003**, *206* (1−4), 314−320.

(15) Mallik, K.; Mandal, M.; Pradhan, N.; Pal, T. Seed mediated formation of bimetallic nanoparticles by uv irradiation: A photochemical approach for the preparation of "core−shell" type structures. *Nano Lett.* **2001**, *1* (6), 319−322.

(16) Jensen, T. R.; Malinsky, M. D.; Haynes, C. L.; Van Duyne, R. P. Nanosphere lithography: Tunable localized surface plasmon resonance spectra of silver nanoparticles. *J. Phys. Chem. B* **2000**, *104* (45), 10549−10556.

(17) Wostek-Wojciechowska, D.; Jeszka, J. K.; Uznanski, P.; Amiens, C.; Chaudret, B.; Lecante, P. Synthesis of gold nanoparticles in solid state by thermal decomposition of an organometallic precursor. *Mater. Sci.-Poland* **2004**, *22* (4), 407−413.

(18) Njagi, E. C.; Huang, H.; Stafford, L.; Genuino, H.; Galindo, H. M.; Collins, J. B.; Hoag, G. E.; Suib, S. L. Biosynthesis of iron and silver nanoparticles at room temperature using aqueous sorghum bran extracts. *Langmuir* **2011**, *27* (1), 264−271.

(19) Lukman, A. I.; Gong, B.; Marjo, C. E.; Roessner, U.; Harris, A. T. Facile synthesis, stabilization, and anti-bacterial performance of discrete Ag nanoparticles using *Medicago sativa* seed exudates. *J. Colloid Interface Sci.* **2011**, *353* (2), 433−444.

(20) Thakkar, K. N.; Mhatre, S. S.; Parikh, R. Y. Biological synthesis of metallic nanoparticles. *Nanomed.: Nanotechnol., Biol. Med.* **2010**, *6* (2), 257−262.

(21) Veerasamy, R.; Xin, T. Z.; Gunasagaran, S.; Xiang, T. F. W.; Yang, E. F. C.; Jeyakumar, N.; Dhanaraj, S. A. Biosynthesis of silver nanoparticles using mangosteen leaf extract and evaluation of their antimicrobial activities. *J. Saudi Chem. Soc.* **2011**, *15* (2), 113−120.

(22) Van Hyning, D. L.; Zukoski, C. F. Formation mechanisms and aggregation behavior of borohydride reduced silver particles. *Langmuir* **1998**, *14* (24), 7034−7046.

(23) Nickel, U.; zu Castell, A.; Pöppl, K.; Schneider, S. A silver colloid produced by reduction with hydrazine as support for highly sensitive surface-enhanced raman spectroscopy. *Langmuir* **2000**, *16* (23), 9087−9091.

(24) Claudio de Santa Maria, L.; Santos, A. L. C.; Oliveira, P. C.; Barud, H. S.; Messaddeq, Y.; Ribeiro, S. J. L. Synthesis and characterization of silver nanoparticles impregnated into bacterial cellulose. *Mater. Lett.* **2009**, *63* (9−10), 797−799.

(25) Harnack, O.; Ford, W. E.; Yasuda, A.; Wessels, J. M. Tris(hydroxymethyl)phosphine-capped gold particles templated by DNA as nanowire precursors. *Nano Lett.* **2002**, *2* (9), 919−923.

(26) Philip, D. *Mangifera Indica* leaf-assisted biosynthesis of well-dispersed silver nanoparticles. *Spectrochim. Acta, Part A* **2011**, *78* (1), 327−331.

(27) Klaus, T.; Joerger, R.; Olsson, E.; Granqvist, C.-G. Silver-based crystalline nanoparticles, microbially fabricated. *Proc. Natl. Acad. Sci. U.S.A.* **1999**, *96* (24), 13611−13614.

(28) Absar, A.; Satyajyoti, S.; Khan, M. I.; Rajiv, K.; Ramani, R.; Srinivas, V.; Murali, S. Intracellular synthesis of gold nanoparticles by a novel alkalotolerant actinomycete, Rhodococcus species. *Nanotechnology* **2003**, *14* (7), 824.

(29) Ahmad, A.; Mukherjee, P.; Senapati, S.; Mandal, D.; Khan, M. I.; Kumar, R.; Sastry, M. Extracellular biosynthesis of silver nanoparticles using the fungus *Fusarium oxysporum*. *Colloids Surf., B* **2003**, *28* (4), 313−318.

(30) Beattie, I. R.; Haverkamp, R. G. Silver and gold nanoparticles in plants: Sites for the reduction to metal. *Metallomics* **2011**, *3* (6), 628−632.

(31) Shankar, S. S.; Rai, A.; Ahmad, A.; Sastry, M. Rapid synthesis of Au, Ag, and bimetallic Au core-Ag shell nanoparticles using Neem (*Azadirachta indica*) leaf broth. *J. Colloid Interface Sci.* **2004**, *275* (2), 496−502.

(32) Gardea-Torresdey, J. L.; Parsons, J. G.; Gomez, E.; Peralta-Videa, J.; Troiani, H. E.; Santiago, P.; Yacaman, M. J. Formation and Growth of Au nanoparticles inside live alfalfa plants. *Nano Lett.* **2002**, *2* (4), 397−401.

(33) Sharma, N. C.; Sahi, S. V.; Nath, S.; Parsons, J. G.; Gardea-Torresde, J. L.; Pal, T. Synthesis of plant-mediated gold nanoparticles and catalytic role of biomatrix-embedded nanomaterials. *Environ. Sci. Technol.* **2007**, *41* (14), 5137−5142.

(34) Song, J.; Kim, B. Biological synthesis of bimetallic Au/Ag nanoparticles using Persimmon (*Diopyros kaki*) leaf extract. *Korean Journal of Chemical Engineering* **2008**, *25* (4), 808−811.

(35) Arunachalam, R.; Dhanasingh, S.; Kalimuthu, B.; Uthirappan, M.; Rose, C.; Mandal, A. B. Phytosynthesis of silver nanoparticles using *Coccinia grandis* leaf extract and its application in the photocatalytic degradation. *Colloids Surf., B* **2012**, *94* (0), 226−230.

(36) Philip, D. Rapid green synthesis of spherical gold nanoparticles using *Mangifera indica* leaf. *Spectrochim. Acta, Part A* **2010**, *77* (4), 807−810.
(37) Kumar, V.; Yadav, S. C.; Yadav, S. K. *Syzygium cumini* leaf and seed extract mediated biosynthesis of silver nanoparticles and their characterization. *J. Chem. Technol. Biotechnol.* **2010**, *85* (10), 1301−1309.
(38) Ganesh Kumar, V.; Dinesh Gokavarapu, S.; Rajeswari, A.; Stalin Dhas, T.; Karthick, V.; Kapadia, Z.; Shrestha, T.; Barathy, I. A.; Roy, A.; Sinha, S. Facile green synthesis of gold nanoparticles using leaf extract of antidiabetic potent *Cassia auriculata*. *Colloids Surf., B* **2011**, *87* (1), 159−163.
(39) Dubey, S. P.; Lahtinen, M.; Särkkä, H.; Sillanpää, M. Bioprospective of *Sorbus aucuparia* leaf extract in development of silver and gold nanocolloids. *Colloids Surf., B* **2010**, *80* (1), 26−33.
(40) Dubey, S. P.; Lahtinen, M.; Sillanpää, M. Green synthesis and characterizations of silver and gold nanoparticles using leaf extract of *Rosa rugosa*. *Colloids Surf., A* **2010**, *364* (1−3), 34−41.
(41) Bar, H.; Bhui, D. K.; Sahoo, G. P.; Sarkar, P.; Pyne, S.; Misra, A. Green synthesis of silver nanoparticles using seed extract of *Jatropha curcas*. *Colloids Surf., A* **2009**, *348* (1−3), 212−216.
(42) Bar, H.; Bhui, D. K.; Sahoo, G. P.; Sarkar, P.; De, S. P.; Misra, A. Green synthesis of silver nanoparticles using latex of *Jatropha curcas*. *Colloids Surf., A* **2009**, *339* (1−3), 134−139.
(43) Das, R. K.; Sharma, P.; Nahar, P.; Bora, U. Synthesis of gold nanoparticles using aqueous extract of *Calotropis procera* latex. *Mater. Lett.* **2011**, *65* (4), 610−613.
(44) Ahmad, N.; Sharma, S.; Alam, M. K.; Singh, V. N.; Shamsi, S. F.; Mehta, B. R.; Fatma, A. Rapid synthesis of silver nanoparticles using dried medicinal plant of basil. *Colloids Surf., B* **2010**, *81* (1), 81−86.
(45) Li, S.; Shen, Y.; Xie, A.; Yu, X.; Qiu, L.; Zhang, L.; Zhang, Q. Green synthesis of silver nanoparticles using *Capsicum annuum* L. extract. *Green Chem.* **2007**, *9* (8), 852−858.
(46) Sheny, D. S.; Mathew, J.; Philip, D. Phytosynthesis of Au, Ag and Au-Ag bimetallic nanoparticles using aqueous extract and dried leaf of *Anacardium occidentale*. *Spectrochim. Acta, Part A* **2011**, *79* (1), 254−262.
(47) Raveendran, P.; Fu, J.; Wallen, S. L. A simple and "green" method for the synthesis of Au, Ag, and Au−Ag alloy nanoparticles. *Green Chem.* **2006**, *8* (1), 34−38.
(48) Kantrud, H. A. *Sago Pondweed (Potamogeton pectinatus L.): A Literature Review*, Version 16JUL97; U.S. Fish and Wildlife Service, Fish and Wildlife Resource Publication 176; Northern Prairie Wildlife Research Center: Jamestown, ND, 1990. http://www.npwrc.usgs.gov/resource/plants/pondweed/index.htm (accessed January 11, 2012).
(49) Boulos, L. *Flora of Egypt*; Al-Hadara Publishing: Egypt, 2005; Vol. *IV*, p 330.
(50) Mhamane, D.; Ramadan, W.; Fawzy, M.; Rana, A.; Dubey, M.; Rode, C.; Lefez, B.; Hannoyer, B.; Ogale, S. From graphite oxide to highly water dispersible functionalized graphene by single step plant extract-induced deoxygenation. *Green Chem.* **2011**, *13* (8), 1990−1996.
(51) Waridel, P.; Wolfender, J.-L.; Lachavanne, J.-B.; Hostettmann, K. Identification of the polar constituents of Potamogeton species by HPLC-UV with post-column derivatization, HPLC-MSn and HPLC-NMR, and isolation of a new ent-labdane diglycoside. *Phytochemistry* **2004**, *65* (16), 2401−2410.
(52) Panda, K. K.; Achary, V. M. M.; Krishnaveni, R.; Padhi, B. K.; Sarangi, S. N.; Sahu, S. N.; Panda, B. B. In vitro biosynthesis and genotoxicity bioassay of silver nanoparticles using plants. *Toxicol. In Vitro* **2011**, *25* (5), 1097−1105.
(53) Das, R. K.; Borthakur, B. B.; Bora, U. Green synthesis of gold nanoparticles using ethanolic leaf extract of *Centella asiatica*. *Mater. Lett.* **2010**, *64* (13), 1445−1447.
(54) Dwivedi, A. D.; Gopal, K. Biosynthesis of silver and gold nanoparticles using *Chenopodium album* leaf extract. *Colloids Surf., A* **2010**, *369* (1−3), 27−33.
(55) Philip, D. Biosynthesis of Au, Ag and Au−Ag nanoparticles using edible mushroom extract. *Spectrochim. Acta, Part A* **2009**, *73* (2), 374−381.
(56) Smitha, S. L.; Philip, D.; Gopchandran, K. G. Green synthesis of gold nanoparticles using *Cinnamomum zeylanicum* leaf broth. *Spectrochim. Acta, Part A* **2009**, *74* (3), 735−739.
(57) Singhal, G.; Bhavesh, R.; Kasariya, K.; Sharma, A.; Singh, R. Biosynthesis of silver nanoparticles using *Ocimum sanctum* (Tulsi) leaf extract and screening its antimicrobial activity. *J. Nanopart. Res.* **2011**, *13* (7), 2981−2988.
(58) Singleton, V. L.; Orthofer, R.; Lamuela-Raventós, R. M.; Lester, P. Analysis of Total Phenols and Other Oxidation Substrates and Antioxidants by Means of Folin-Ciocalteu Reagent. In *Methods in Enzymology*; Academic Press: Waltham, MA, 1999; Vol. *299*, pp 152−178.
(59) Everette, J. D.; Bryant, Q. M.; Green, A. M.; Abbey, Y. A.; Wangila, G. W.; Walker, R. B. Thorough study of reactivity of various compound classes toward the folin-ciocalteu reagent. *J. Agric. Food Chem.* **2010**, *58* (14), 8139−8144.
(60) Ferreira, I. C. F. R.; Baptista, P.; Vilas-Boas, M.; Barros, L. Free-radical scavenging capacity and reducing power of wild edible mushrooms from northeast Portugal: Individual cap and stipe activity. *Food Chem.* **2007**, *100* (4), 1511−1516.
(61) Yang, Y.; Shi, J.; Kawamura, G.; Nogami, M. Preparation of Au-Ag, Ag-Au core-shell bimetallic nanoparticles for surface-enhanced Raman scattering. *Scr. Mater.* **2008**, *58* (10), 862−865.
(62) Prathap Chandran, S.; Ghatak, J.; Satyam, P. V.; Sastry, M. Interfacial deposition of Ag on Au seeds leading to $Au_{core}Ag_{shell}$ in organic media. *J. Colloid Interface Sci.* **2007**, *312* (2), 498−505.
(63) Kora, A. J.; Sashidhar, R. B.; Arunachalam, J. Aqueous extract of gum olibanum (*Boswellia serrata*): A reductant and stabilizer for the biosynthesis of antibacterial silver nanoparticles. *Process Biochem.* **2012**, *47* (10), 1516−1520.
(64) Link, S.; Wang, Z. L.; El-Sayed, M. A. Alloy formation of gold-silver nanoparticles and the dependence of the plasmon absorption on their composition. *J. Phys. Chem. B* **1999**, *103* (18), 3529−3533.
(65) Philip, D. Green synthesis of gold and silver nanoparticles using *Hibiscus rosa sinensis*. *Phys. E* **2010**, *42* (5), 1417−1424.
(66) Kouvaris, P.; Delimitis, A.; Zaspalis, V.; Papadopoulos, D.; Tsipas, S. A.; Michailidis, N. Green synthesis and characterization of silver nanoparticles produced using *Arbutus Unedo* leaf extract. *Mater. Lett.* **2012**, *76*, 18−20.
(67) Dubey, S. P.; Lahtinen, M.; Sillanpää, M. Tansy fruit mediated greener synthesis of silver and gold nanoparticles. *Process Biochem.* **2010**, *45* (7), 1065−1071.
(68) Philip, D.; Unni, C.; Aromal, S. A.; Vidhu, V. K. Murraya Koenigii leaf-assisted rapid green synthesis of silver and gold nanoparticles. *Spectrochim. Acta, Part A* **2011**, *78* (2), 899−904.
(69) Cruz, D.; Falé, P. L.; Mourato, A.; Vaz, P. D.; Luisa Serralheiro, M.; Lino, A. R. L. Preparation and physicochemical characterization of Ag nanoparticles biosynthesized by *Lippia citriodora* (Lemon Verbena). *Colloids Surf., B* **2010**, *81* (1), 67−73.
(70) Aswathy Aromal, S.; Philip, D. Green synthesis of gold nanoparticles using *Trigonella foenum-graecum* and its size-dependent catalytic activity. *Spectrochim. Acta, Part A* **2012**, *97*, 1−5.
(71) Edison, T. J. I.; Sethuraman, M. G. Instant green synthesis of silver nanoparticles using *Terminalia chebula* fruit extract and evaluation of their catalytic activity on reduction of methylene blue. *Process Biochem.* **2012**, *47* (9), 1351−1357.
(72) Sheny, D. S.; Mathew, J.; Philip, D. Synthesis characterization and catalytic action of hexagonal gold nanoparticles using essential oils extracted from *Anacardium occidentale*. *Spectrochim. Acta, Part A* **2012**, *97*, 306−310.
(73) Vijayakumar, M.; Priya, K.; Nancy, F. T.; Noorlidah, A.; Ahmed, A. B. A. Biosynthesis, characterisation and anti-bacterial effect of plant-mediated silver nanoparticles using *Artemisia nilagirica*. *Ind. Crops Prod.* **2013**, *41*, 235−240.
(74) MubarakAli, D.; Thajuddin, N.; Jeganathan, K.; Gunasekaran, M. Plant extract mediated synthesis of silver and gold nanoparticles

and its antibacterial activity against clinically isolated pathogens. *Colloids Surf., B* **2011**, *85* (2), 360−365.
(75) Kaviya, S.; Santhanalakshmi, J.; Viswanathan, B.; Muthumary, J.; Srinivasan, K. Biosynthesis of silver nanoparticles using citrus sinensis peel extract and its antibacterial activity. *Spectrochim. Acta, Part A* **2011**, *79* (3), 594−598.
(76) Rajakumar, G.; Abdul Rahuman, A. Larvicidal activity of synthesized silver nanoparticles using *Eclipta prostrata* leaf extract against filariasis and malaria vectors. *Acta Trop.* **2011**, *118* (3), 196−203.
(77) Roopan, S. M.; Rohit; Madhumitha, G.; Rahuman, A. A.; Kamaraj, C.; Bharathi, A.; Surendra, T. V. Low-cost and eco-friendly phyto-synthesis of silver nanoparticles using *Cocos nucifera* coir extract and its larvicidal activity. *Ind. Crops Prod.* **2013**, *43*, 631−635.
(78) Wang, Y.; He, X.; Wang, K.; Zhang, X.; Tan, W. Barbated skullcup herb extract-mediated biosynthesis of gold nanoparticles and its primary application in electrochemistry. *Colloids Surf., B* **2009**, *73* (1), 75−79.
(79) Liu, J.-H.; Wang, A.-Q.; Chi, Y.-S.; Lin, H.-P.; Mou, C.-Y. Synergistic effect in an Au−Ag alloy nanocatalyst: CO oxidation. *J. Phys. Chem. B* **2004**, *109* (1), 40−43.
(80) Endo, T.; Yoshimura, T.; Esumi, K. Synthesis and catalytic activity of gold−silver binary nanoparticles stabilized by PAMAM dendrimer. *J. Colloid Interface Sci.* **2005**, *286* (2), 602−609.
(81) Wang, A.-Q.; Chang, C.-M.; Mou, C.-Y. Evolution of catalytic activity of Au−Ag bimetallic nanoparticles on mesoporous support for CO oxidation. *J. Phys. Chem. B* **2005**, *109* (40), 18860−18867.
(82) Wang, A.-Q.; Liu, J.-H.; Lin, S. D.; Lin, T.-S.; Mou, C.-Y. A novel efficient Au−Ag alloy catalyst system: Preparation, activity, and characterization. *J. Catal.* **2005**, *233* (1), 186−197.